Supplementary material

Overcoming surface energy to control Cu_3N epitaxial growth

Zainab Fatima[1], Isao Ohkubo[1,3,*], Satoshi Ishii[1,3], Takahiro Nagata[2], Takashi Aizawa[1], Takao Mori[1,3]

[1.] Research Center for Materials Nanoarchitectonics (MANA), National Institute for Materials Science (NIMS), 1-1 Namiki, Tsukuba, Ibaraki 305-0044, Japan

[2.] Research Center for Electronic and Optical Materials, National Institute for Materials Science (NIMS), 1-1 Namiki, Tsukuba, Ibaraki 305-0044, Japan

[3.] Department of Materials Science, Institute of Pure and Applied Sciences, University of Tsukuba, 1-1-1 Tennodai, Tsukuba, Ibaraki 305-8573, Japan

[*] Author to whom correspondence should be addressed: OHKUBO.Isao@nims.go.jp

(1) Auger electron spectra and atomic force microscope image of Cu_3N thin films

Chemical depth analysis of Cu_3N thin films using Auger electron spectroscopy (AES) is portrayed in Fig. S1. Cu *LMM* and *MVV* peaks, carbon (approx. 268 eV, *KLL* transition), and oxygen (approx. 520 eV, *KLL* transition) peaks were detected for the non-sputtered Cu_3N surfaces. These peaks might originate from a surface contamination layer of physisorbed organic and water molecules. Very weak carbon and oxygen peaks remain even after prolonged sputter etching. As portrayed in an atomic force microscopy (AFM) image of the Cu_3N thin film surface in Fig. S2, rough surfaces comprising granular domains with several hundred nanometers' size were observed. Consequently, the origins of these carbon and oxygen peaks in the AES spectra of sputtered surfaces are regarded as residual carbon and oxygen in the depressions of Cu_3N thin film surfaces. This AFM image suggests that large quantities of nuclei formed because of the high-energy supply species in the reactive DC sputtering method and because of the low growth temperature of less than 200 °C. Nitrogen peaks were extremely weak or undetectable. This result is consistent with findings from ex-situ X-ray photoelectron spectroscopy (XPS) measurements of Cu_3N thin films prepared using the RF magnetron sputtering method, as reported by Richthofen et al.[S1] Their study detected no nitrogen XPS peak in either as-supplied (non-sputtered) or Ar^+-sputtered Cu_3N thin film samples, perhaps because Cu_3N is a low-stability compound with a low decomposition temperature of 260 °C. That result is regarded as attributable to selective etching of light-element nitrogen atoms near the Cu_3N thin film surfaces by irradiation of high-energy Kr^+ or Ar^+ ions.

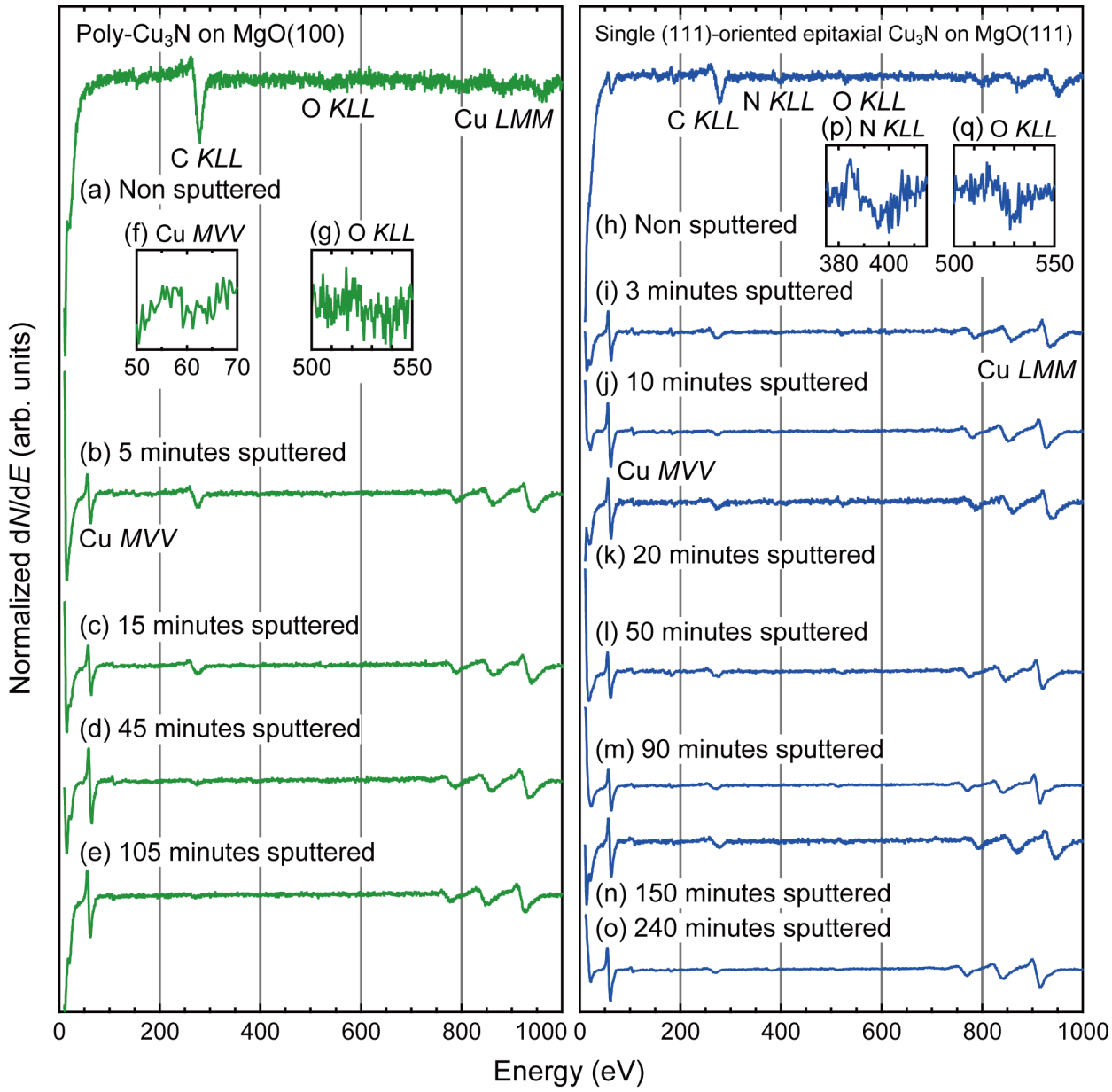

Fig. S1. Auger electron spectra of (a)–(g) polycrystalline Cu_3N thin film grown on a MgO(100) substrate and of single (111)-oriented Cu_3N epitaxial thin film grown on a MgO(111) substrate. (f),(g),(p), and (q) enlarged Auger electron spectra of Cu *MVV*, N *KLL*, and O *KLL* peaks for the non-sputtered Cu_3N surfaces. The d*N*/d*E* values of each Auger electron spectrum are normalized by the Cu peak at around 920 eV (*LMM* transition) to support discussion based on the d*N*/d*E* ratio of AES peaks.

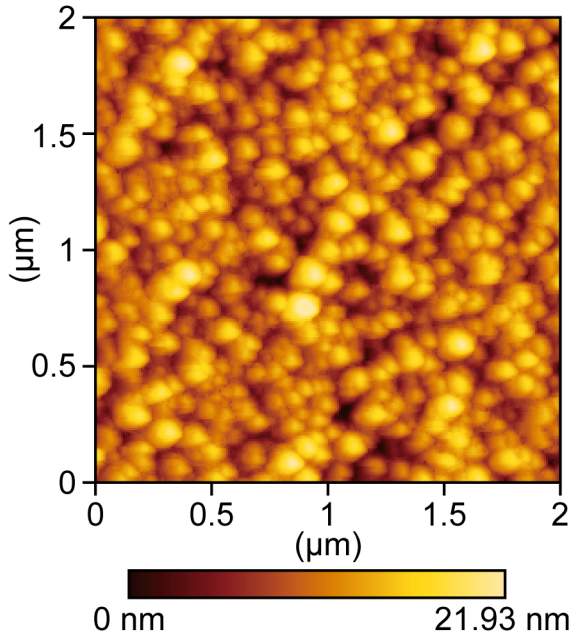

Fig. S2. Atomic force microscopy image of a single (111)-oriented Cu_3N epitaxial thin film grown on a MgO(111) substrate.

(2) Thermochemical cycles and formation enthalpies for bond energy calculations

Table S1. Thermochemical cycles and formation enthalpies (ΔH_f°) used for bond energy (D°) calculations

Thermochemical cycle [a]	ΔH_f° (298.15 K) (kJ/mol)
Cu_3N (*CN*=2, D°=253.53 kJ/mol)	
$1/2N_2(g)\rightarrow N(g)$	472.7 [b]
$Cu(cr)\rightarrow Cu(g)$	338.32 [b]
$3Cu(cr)+1/2N_2(g)\rightarrow Cu_3N(cr)$	74.5 [b]
$Cu_3N(cr)\rightarrow 3Cu(g)+N(g)$	1413.15 [c]
MgO (*CN*=6, D°=166.43 kJ/mol)	
$1/2O_2(g)\rightarrow O(g)$	249.17 [b]
$Mg(cr)\rightarrow Mg(g)$	147.7 [b]
$Mg(cr)+1/2O_2(g)\rightarrow MgO(cr)$	-601.7 [b]
$MgO(cr)\rightarrow Mg(g)+O(g)$	998.57 [c]
sapphire (α-Al_2O_3) (*CN*=6, D°=256.33 kJ/mol)	
$1/2O_2(g)\rightarrow O(g)$	249.17 [b]
$Al(cr)\rightarrow Al(g)$	326.4 [b]
$2Al(cr)+3/2O_2(g)\rightarrow Al_2O_3(cr)$	-1675.7 [b]
$Al_2O_3(cr)\rightarrow 2Al(g)+3O(g)$	3076.01 [c]
$SrTiO_3$ (*CN*=6 for Ti, *CN*=12 for Sr, D°=167.6 kJ/mol for Sr-O, 318.82 kJ/mol for Ti-O)	
$1/2O_2(g)\rightarrow O(g)$	249.17 [b]
$Ti(cr)\rightarrow Ti(g)$	469.9 [b]
$Ti(cr)+O_2(g)\rightarrow TiO_2(cr)$	-944.7 [b]
$TiO_2(cr)\rightarrow Ti(g)+2O(g)$	1912.94 [c]
$Sr(cr)\rightarrow Sr(g)$	164.4 [b]
$Sr(cr)+1/2O_2(g)\rightarrow SrO(cr)$	-592.0 [b]
$SrO(cr)\rightarrow Sr(g)+O(g)$	1005.57 [c]
$Sr(cr)+Ti(cr)+3/2O_2(g)\rightarrow SrTiO_3(cr)$	-1672.39 [b]
$SrTiO_3(cr)\rightarrow Sr(g)+Ti(g)+3O(g)$	3054.2 [c]

[a] *CN*, coordination number of metal cation; cr, crystalline solid; g, gaseous. [b] Values of ΔH_f° were referred from Ref. 44. [c] Obtained using thermochemical calculations.

(3) Growth rate of Cu_3N thin films shown as a function of growth temperature

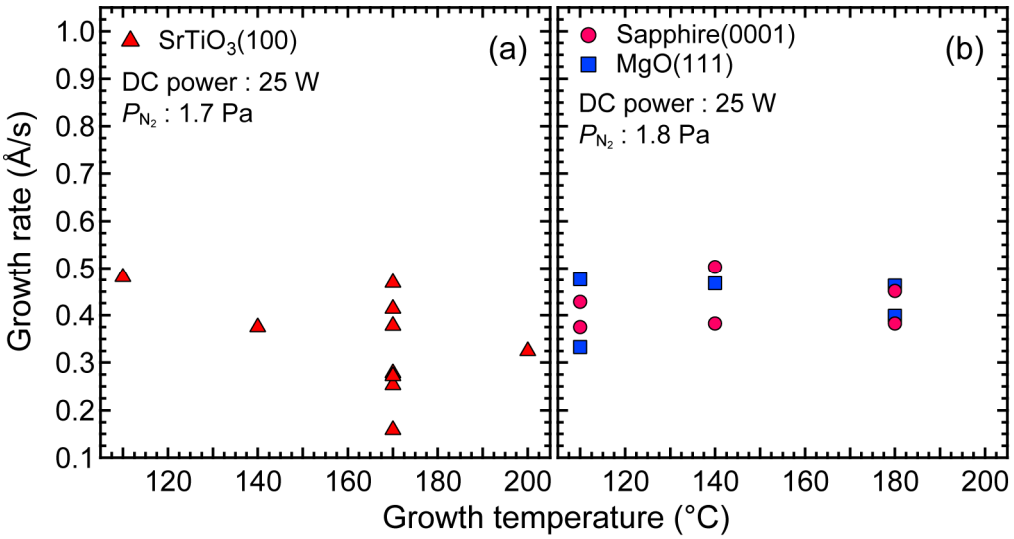

Fig. S3. Growth rate of Cu_3N thin films grown under specific conditions shown as a function of growth temperature: (a) grown on cubic symmetry surface unit cell substrates of MgO(100) and $SrTiO_3$(100) under the conditions of 25 W DC power and 1.7 Pa nitrogen gas pressure (P_{N_2}), and (b) grown on rhombohedral symmetry surface unit cell substrates of sapphire(0001) and MgO(111) under conditions of 25 W DC power and 1.8 Pa nitrogen gas pressure.

(4) XRD 2θ–ω patterns of a Cu_3N(111) epitaxial thin film grown on a MgO(111) substrate, and of a bare MgO(111) substrate

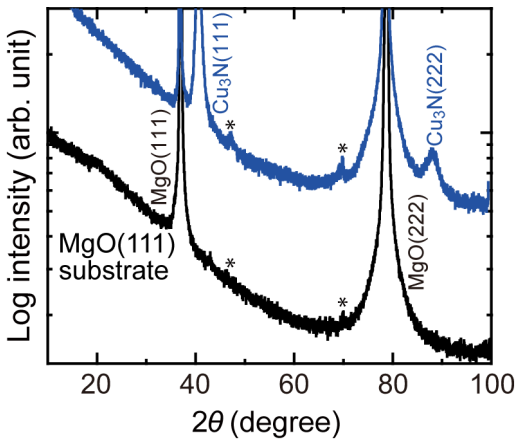

Fig. S4. XRD 2θ–ω patterns of a Cu_3N(111) epitaxial thin film grown on a MgO(111) substrate (blue) and a bare MgO(111) substrate (black). The bare MgO(111) substrate is presented for reference, showing that peaks originate from the substrate.

(5) Electronic band structures of Cu_3N calculated using the mBJ exchange potential and GGA-PBE exchange-correlation functional

Figure S5 portrays the electronic band structures of Cu_3N calculated using modified Becke–Johnson potential (mBJ) and generalized gradient approximation Perdew–Burke–Ernzerhof (GGA-PBE) exchange-correlation functional. Table S2 presents energy level values of conduction band minimum (CBM) and valence band maximum (VBM) at each Brillouin zone point in the Cu_3N electronic band structures, in addition to energy band gap values for each combination of Brillouin zone points. For mBJ, the energy level at the Γ point (CBM) is lower than that at the R point, whereas the energy level at the Γ point is higher than that at the R point for GGA-PBE. The band structures differ because of differences in the exchange-correlation functional. Changes in band structures attributable to functional differences have been described in several reports of the literature.[58–63] Consequently, these differences in energy band gap values between optical measurements and DFT calculations might be attributable to the computational method, in addition to the measurement and analysis accuracies and errors in spectroscopic ellipsometry measurements.

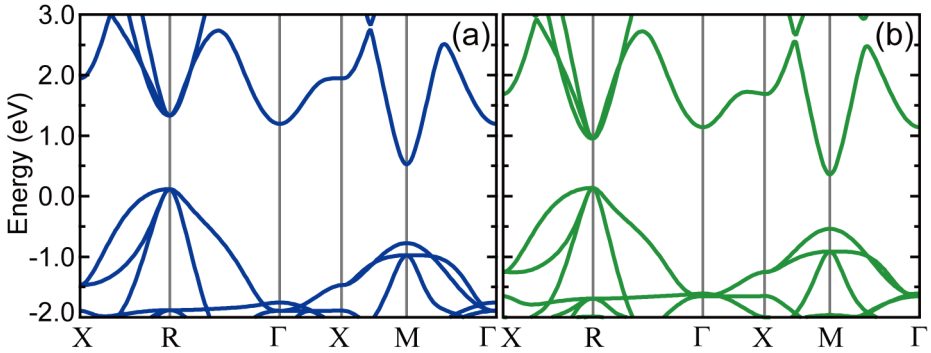

Fig. S5. Electronic band structures of Cu_3N obtained using DFT calculation with (a) mBJ exchange potential and (b) GGA-PBE exchange-correlation functional. Labels in the Brillouin zone of electronic band structure Γ, X, R, and M respectively correspond to the following in lattice constant units: 0,0,0; 1,0,0; 1,1,1; and 1,0,1.

Table S2. Energy levels of the conduction band minimum and valence band maximum at each point in the Brillouin zone of the electronic band structures of Cu_3N, and energy band gap values between points in the Brillouin zone.

	Conduction band minimum (CBM) (eV)			Valence band maximum (VBM) (eV)		Energy band gap (eV)		
	R	Γ	M	R	M	R(CBM)-R(VBM)	Γ(CBM)-R(VBM)	M(CBM)-R(VBM)
mBJ	1.329	1.195	0.525	0.117	-0.773	1.211	1.078	0.408
GGA-PBE	0.951	1.140	0.355	0.138	-0.538	0.813	1.003	0.217

(6) References for supplementary material

S1. A. von Richthofen, R. Domnick, and R. Cremer, "Cu-N films grown by reactive MSIP: Constitution, structure and morphology," Mikrochim. Acta **125**, 173–177 (1997).